Acta Crystallographica Section A
Foundations of Crystallography
ISSN 0108-7673

Received 8 November 2005
Accepted 29 August 2006

Finite size effects of nanoparticles on the atomic pair distribution functions

Katsuaki Kodama,* Satoshi Iikubo, Tomitsugu Taguchi and Shin-ichi Shamoto

Quantum Beam Science Directorate, Japan Atomic Energy Agency, Tokai, Ibaraki 319-1195, Japan. Correspondence e-mail: kodama.katsuaki@jaea.go.jp

The finite size effects of nanoparticles on the atomic pair distribution functions (PDF) are discussed by calculating the radial distribution functions (RDF) on nanoparticles with various shapes, such as sheet, belt, rod, tube and sphere, assuming continua. Their characteristics are shown depending on the shapes and the sizes of the nanoparticles. The formulas of a PDF analysis which take account of such effects are presented and are found to reproduce the experimental data.

1. Introduction

Many types of nanoparticles have been synthesized and studied on their physical and chemical properties. The nanoparticles may exhibit exotic physical properties, which can be different from those of the bulk materials, owing to their finite sizes and their large volume fraction of the surface atoms. The atomic scale crystal structures of nanoparticles give us information to help in understanding their properties. However, it is hard to determine their structures by ordinary techniques used for bulk materials, for example, traditional Rietveld analysis. In the cases of nanoparticles, the diffraction patterns mainly consist of diffuse broad peaks because the periodicity of their unit cells is limited to nanoscale.

The technique of atomic pair distribution function (PDF) analysis can be applied to the determination of the local structure of nanoparticles. For the system composed of one kind of atom, the number of pair atoms in a shell of thickness dr at distance r from another one are obtained as $R(r)\,dr$, where $R(r)$ is the radial distribution function (RDF). $R(r)$ is related to the reduced pair distribution function $G(r)$ *via* the pair distribution function $g(r)$ as follows (Egami & Billinge, 2003).

$$g(r) = R(r)/4\pi r^2\rho_0, \quad (1)$$

$$G(r) = 4\pi r\rho_0[g(r) - 1], \quad (2)$$

where ρ_0 is a number density of atoms in the sample. Experimentally, $G(r)$ can be obtained from the total scattering measurement, generally on a powder sample. $G(r)$ is determined from the structure function $S(Q)$ of the total scattering, *via* Fourier transformation as follows.

$$G(r) = (2/\pi)\int Q[S(Q) - 1]\sin(Qr)\,dQ, \quad (3)$$

where Q is the magnitude of the scattering wavevector and $S(Q)$ is the data for the sample with no preferred orientation in an ideal case. In the cases of amorphous materials and nanoparticles, even if $S(Q)$ does not have any well defined peaks as mentioned above, $G(r)$ can have sharp peaks, at least in the small-r region. Then the PDF analysis is applicable to the structural analysis of the materials with only short-range correlation. Recently, the technique of PDF has been applied to the determination of the structure of nanoparticles (Mckenzie *et al.*, 1992; Gilbert *et al.*, 2004; Petkov *et al.*; 2004; Gateshki *et al.*, 2004).

So far, the effects of the shape and finite size of a nanoparticle, however, have not been considered in the PDF analysis. The atomic correlation remains only in the size and, as a result, $G(r)$ does not have any peak in the longer-r region than the particle size if there is no correlation between nearby particles. Actually, $G(r)$ of C_{60} shows sharp peaks at r shorter than the diameter of the C_{60} molecule while, at r longer than the diameter, $G(r)$ has only weak broad peaks corresponding to the correlation between the molecules (Egami & Billinge, 2003). Furthermore, the peak intensities of the PDF must be reduced with increasing r, in comparison with those of the bulk sample. So the distribution functions modified by their sizes and shapes need to be used for the detailed structural analyses of nanoparticles.

Such a detailed analysis gives other structural information on the nanoparticle. The nanoparticle of zinc sulfide is analyzed by PDF with the spherical shape effect (Gilbert *et al.*, 2004). After they determined the average size and the shape of the nanoparticle by means of small-angle X-ray scattering and ultraviolet–visible absorption spectroscopy, they discussed the disorder and the strain in the nanoparticle from the difference between the average size and the local correlation size by PDF. The corrections for the size and shape effects are crucial to a discussion of the local lattice disorder in the nanoparticle.

In this paper, we calculate the RDFs of the various nanoparticles by assuming that they are continua, for the corrections of the size and shape effects, and obtain the correction factor to the RDFs and the reduced PDFs for the various nanoparticles. We present formulas of PDFs including the correction factor and apply the formula to the experimental data of TiO_2 nanoparticle, as an example.

2. Calculations of radial distribution functions and correction factors on nanoparticles

2.1. Calculation method

In the calculation of the radial distribution function $R(r)$ of a nanoparticle, we consider the atomic pair distribution only in the particle and assume that the atomic number density is zero (vacuum) outside the particle. The atomic number density in the nanoparticle is ρ_0'. The RDF of a three-dimensional continuum with infinite size is given as $R_\infty(r) = 4\pi r^2 \rho_0'$, as mentioned in §2.2. So the RDF of the nanoparticle, $R_{\rm nano}(r)$, is modified by the correction factor $f(r)$, which is defined as

$$f(r) = R_{\rm nano}(r)/R_\infty(r). \tag{4}$$

When $r \to 0$, $f(r)$ must be unity, and, when r is longer than the size of the nanoparticle or $r \to \infty$, $f(r)$ becomes zero. This factor can be regarded as a kind of particle form factor instead of the well known atomic form factor.

In this paper, we assume that nanoparticles are randomly oriented to the incident beam, resulting in no preferred orientation effect to the structure function $S(Q)$.

In the real analysis, the pair distribution between the particles should be considered. The formulation including the pair distribution between particles will be discussed in the next section.

2.2. Simple case

In this section, we take up simple cases and discuss the effect of the dimensionality of a particle to the radial distribution function. First, we consider the wire with an infinitesimal thickness shown in Fig. 1(*a*). The density in this wire is defined as $\rho_{0,1\rm D}'$, whose dimension is an inverse of the length. Here we assume that r is much shorter than the length of the wire L. The number of atoms in a length dr at a distance r from an atom at the origin (O) is $2\rho_{0,1D}'\,{\rm d}r$, as shown in the figure. Then the RDF is obtained as

$$R_{\rm 1D}(r) = 2\rho_{0,\rm 1D}'. \tag{5}$$

In the case of the sheet with an infinitesimal thickness shown in Fig. 1(*b*), if $r \ll L$, atoms paired with an atom at the origin O are in the ring with radius r and thickness dr, which is shown by the bold line in Fig. 1(*b*). So $R_{\rm 2D}(r)$ is given by

$$R_{\rm 2D}(r) = 2\pi r \rho_{0,\rm 2D}'. \tag{6}$$

In the case of the three-dimensional block shown in Fig. 1(*c*), paired atoms are in the spherical shell with a radius r and a thickness dr, and $R_{\rm 3D}(r)$ is given by

$$R_{\rm 3D}(r) = 4\pi r^2 \rho_{0,\rm 3D}'. \tag{7}$$

In the cases of one-, two- and three-dimensional nanoparticles, RDFs have r constant, r linear and r squared dependences, respectively.

Next, we calculate the RDF of the nanobelt with a width a and an infinitesimal thickness which is shown in Fig. 1(*d*) as an example of a typical nanoparticle. Here, it is assumed that $r \ll L$. In this case, we consider the number of atoms in an annulus of thickness dr at a distance r from an atom at a position P which is distant from the edge of the belt by p, as shown in the figure. It is given by $R(r, p)\,{\rm d}r$. So $R(r, p)$ can be regarded as the 'partial radial distribution function' (PRDF) at p. $R(r)$ is given by $\int_0^a R(r, p)\,{\rm d}p/a$. If $r \le a/2$, $R(r, p)$ is proportional to the length of the circumference for $r \le p \le a - r$, and it is proportional to the length of the arcs with interior angles of $2\pi - 2\theta$ for $p \le r$ and $2\pi - 2\theta'$ for $a - r \le p \le a$, where $\theta = \arccos(p/r)$ and $\theta' = \arccos[(a - p)/r]$. So

$$R_{\rm 2Dbelt}(r) = \left[\int_0^r (2\pi - 2\theta) r\,{\rm d}p + \int_r^{a-r} 2\pi r\,{\rm d}p + \int_{a-r}^{a} (2\pi - 2\theta') r\,{\rm d}p\right]\rho_{0,\rm 2D}'/a.$$

In the case of $a/2 \le r \le a$, $R(r, p)$ is proportional to the length of the arcs with interior angles of $2\pi - 2\theta$ for $p \le a - r$ and $2\pi - 2\theta'$ for $r \le p \le a$. At the other p, $R(r, p)$ is proportional to the length of the bold line shown in Fig. 1(*d*). Then

$$R_{\rm 2Dbelt}(r) = \left[\int_0^{a-r} (2\pi - 2\theta) r\,{\rm d}p + \int_{a-r}^{r} (2\pi - 2\theta - 2\theta') r\,{\rm d}p + \int_r^a (2\pi - 2\theta') r\,{\rm d}p\right]\rho_{0,\rm 2D}'/a.$$

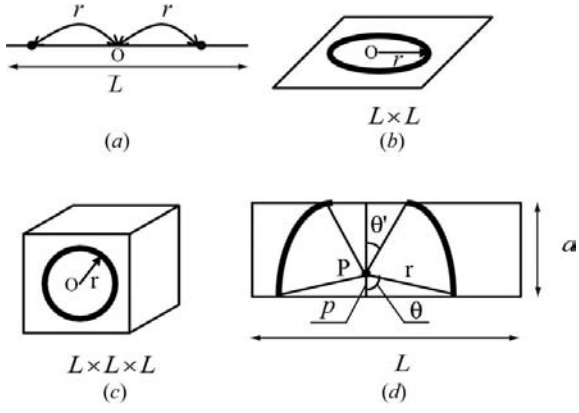

Figure 1
Schematic diagram of (*a*) one-dimensional, (*b*) two-dimensional and (*c*) three-dimensional particles, and (*d*) a nanobelt.

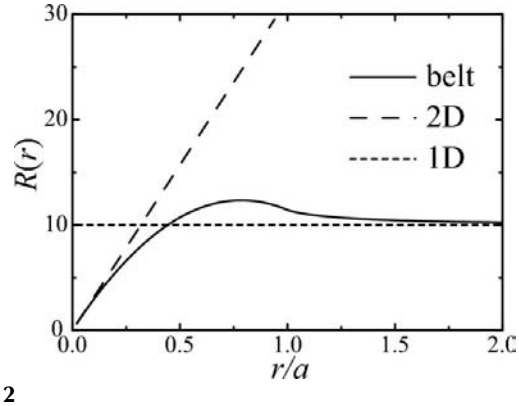

Figure 2
The radial distribution functions of the wire (1D), the sheet (2D) and the nanobelt.

Since, for $r \geq a$, $R(r, p)$ is obtained by the bold line for all p,

$$R_{\rm 2Dbelt}(r) = \left[\int_0^a (2\pi - 2\theta - 2\theta')r\,{\rm d}p\right]\rho'_{0,2D}/a.$$

By calculating the above integrations, we obtain the RDF of the nanobelt as follows.

$$R_{\rm 2Dbelt}(r) = \begin{cases} (2\pi ar - 4r^2)\rho'_{0,2D}/a & (r \leq a) \\ \left[2\pi ar - 4r^2 - 4ar\arccos\left(\frac{a}{r}\right) \right. & \\ \quad \left. + 4r(r^2 - a^2)^{1/2}\right]\rho'_{0,2D}/a & (r \geq a). \end{cases} \quad (8)$$

When r is much shorter than a, $R_{\rm 2Dbelt} \sim 2\pi r\rho'_{0,2D}$, which is equal to $R_{\rm 2D}(r)$. For $r \gg a$, $R_{\rm 2Dbelt} \sim 2a\rho'_{0,2D}$, equal to $R_{\rm 1D}(r)$. The calculated $R(r)$ of the nanobelt is shown in Fig. 2. Here, we use the parameter $\rho'_{0,2D} = 1$. The RDFs of the wire and the sheet are also plotted in the figure, assuming the same atomic densities. For $r \to 0$, the RDF of the nanobelt approaches the RDF of the two-dimensional sheet and, for $r \gg a$, it merges into that of the wire. We know the dimensional dependence of RDF by such simple calculations.

2.3. Nanosheet

In this subsection, we consider a realistic model. First, we take up the nanosheet with a thickness of t as shown in Fig. 3. The area is $L \times L$ and it is assumed that $r \ll L$. The atomic number density in the sheet is $\rho'_{0,3D}$. Here, we also consider the PRDF at p, $R(r, p)$, where p is the distance from the bottom wall of the sheet to the center of the sphere with a radius r, as shown in Fig. 3(b). $R(r, p)$ is obtained as product of $\rho'_{0,3D}$ and the volume of the overlapping part of the sheet and the spherical shell with a radius r and a thickness dr, shown by the bold line in the figure. $R_{\rm sheet}(r)$ is given by $\int_0^t R(r, p)\,{\rm d}p/t$. In the case of $r \leq t/2$, $R(r, p)$ is given as the number of atoms in the complete spherical shell for $r \leq p \leq t - r$. $R(r, p)$ is proportional to the surface area of the object obtained by rotating the fan with an interior angle θ and θ' for $p \leq r$ and $t - r \leq p \leq t$, respectively, where $\theta = \arccos(p/r)$ and $\theta' = \arccos[(t - p)/r]$. Then, for $r \leq t/2$,

$$R_{\rm sheet}(r) = \left[\int_0^r 2\pi r^2\left(1 + \frac{p}{r}\right){\rm d}p + \int_r^{t-r} 4\pi r^2\,{\rm d}p + \int_{t-r}^t 2\pi r^2\left(1 + \frac{t-p}{r}\right){\rm d}p\right]\rho'_{0,3D}/t.$$

In the case of $t/2 \leq r \leq t$, $R(r, p) = 2\pi r^2(1 + p/r)\rho'_{0,3D}$ for $p \leq t - r$ and $R(r, p) = 2\pi r^2[1 + (t - p)/r]\rho'_{0,3D}$ for $r \leq p \leq t$. For $t - r \leq p \leq r$, $R(r, p)$ is given as a product of $\rho'_{0,3D}$ and the surface area of the object obtained by rotating the bold line shown in Fig. 3(b). For $t/2 \leq r \leq t$,

$$R_{\rm sheet}(r) = \left[\int_0^{t-r} 2\pi r^2\left(1 + \frac{p}{r}\right){\rm d}p + \int_{t-r}^r 2\pi rt\,{\rm d}p + \int_r^t 2\pi r^2\left(1 + \frac{t-p}{r}\right){\rm d}p\right]\rho'_{0,3D}/t.$$

Since, in the case of $r \geq t$, $R(r, p) = 2\pi rt$ for all p,

$$R_{\rm sheet}(r) = \int_0^t 2\pi rt\,{\rm d}p\,\rho'_{0,3D}/t.$$

By calculating the above integrations, we finally obtain the RDF of the nanosheet as follows.

$$R_{\rm sheet}(r) = \begin{cases} (4\pi r^2 t - 2\pi r^3)\rho'_{0,3D}/t & (r \leq t) \\ 2\pi tr\rho'_{0,3D} & (r \geq t). \end{cases} \quad (9)$$

Fig. 4(a) shows the RDF calculated on the nanosheet. In the calculations, the atomic number density in the nanosheet $\rho'_{0,3D}$ is unity. For $r \ll t$, the RDFs are proportional to r^2. This r dependence corresponds with the case of the three-dimen-

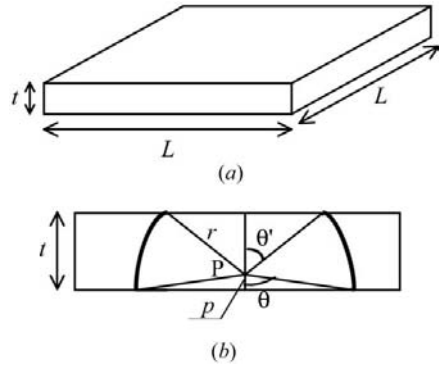

Figure 3
(a) Three-dimensional scheme of a nanosheet with thickness t. (b) The sectioned diagram of the nanosheet.

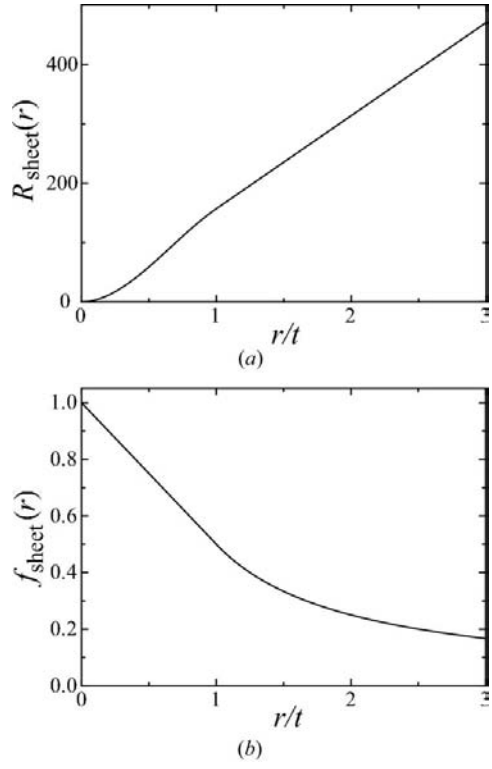

Figure 4
(a) The radial distribution function and (b) the correction factor for the nanosheet with thickness t.

Table 1
Integral ranges of the left side (L1, L2 and L3) for various conditions of the relations between r, t, a, p and q.

Conditions	L1	L2	L3
(i) $r \le p$			
$r \le q \le t - r$	$\int_{-r}^{r} \mathrm{d}x$		
$q \le t - r, q \ge r$	$\int_{-r}^{t-q} \mathrm{d}x$		
$q \le t - r, q \le r$	$\int_{-q}^{r} \mathrm{d}x$		
$t - r \le q \le r$	$\int_{-q}^{t-q} \mathrm{d}x$		
(ii) $r > p$			
$t - (r^2 - p^2)^{1/2} < q < (r^2 - p^2)^{1/2}$		$\int_{-q}^{t-q} \mathrm{d}x$	
$(r^2 - p^2)^{1/2} < q < r$ and $q > t - (r^2 - p^2)^{1/2}$	$\int_{-q}^{-(r^2-p^2)^{1/2}} \mathrm{d}x$	$\int_{-(r^2-p^2)^{1/2}}^{t-q} \mathrm{d}x$	
$q > r, q > t - (r^2 - p^2)^{1/2}$	$\int_{-r}^{-(r^2-p^2)^{1/2}} \mathrm{d}x$	$\int_{-(r^2-p^2)^{1/2}}^{t-q} \mathrm{d}x$	
$q < (r^2 - p^2)^{1/2}$ and $q < t - r$		$\int_{-q}^{(r^2-p^2)^{1/2}} \mathrm{d}x$	$\int_{(r^2-p^2)^{1/2}}^{r} \mathrm{d}x$
$q < (r^2 - p^2)^{1/2}$ and $t - q \le q \le t - (r^2 - p^2)^{1/2}$		$\int_{-q}^{(r^2-p^2)^{1/2}} \mathrm{d}x$	$\int_{(r^2-p^2)^{1/2}}^{t-q} \mathrm{d}x$
$r < q < t - r$	$\int_{-r}^{-(r^2-p^2)^{1/2}} \mathrm{d}x$	$\int_{-(r^2-p^2)^{1/2}}^{(r^2-p^2)^{1/2}} \mathrm{d}x$	$\int_{(r^2-p^2)^{1/2}}^{r} \mathrm{d}x$
$q > r$ and $t - r < q < t - (r^2 - p^2)^{1/2}$	$\int_{-r}^{-(r^2-p^2)^{1/2}} \mathrm{d}x$	$\int_{-(r^2-p^2)^{1/2}}^{(r^2-p^2)^{1/2}} \mathrm{d}x$	$\int_{(r^2-p^2)^{1/2}}^{t-q} \mathrm{d}x$
$(r^2 - p^2)^{1/2} < q < r$ and $q < t - r$	$\int_{-q}^{-(r^2-p^2)^{1/2}} \mathrm{d}x$	$\int_{-(r^2-p^2)^{1/2}}^{(r^2-p^2)^{1/2}} \mathrm{d}x$	$\int_{(r^2-p^2)^{1/2}}^{r} \mathrm{d}x$
$(r^2 - p^2)^{1/2} < q < r$ and $t - r < q < t - (r^2 - p^2)^{1/2}$	$\int_{-q}^{-(r^2-p^2)^{1/2}} \mathrm{d}x$	$\int_{-(r^2-p^2)^{1/2}}^{(r^2-p^2)^{1/2}} \mathrm{d}x$	$\int_{(r^2-p^2)^{1/2}}^{t-q} \mathrm{d}x$

sional particle mentioned in §2.2. For $r > t$, $R_{\mathrm{sheet}}(r) \propto r$, corresponding with $R_{\mathrm{2D}}(r)$. The correction factor $f_{\mathrm{sheet}}(r)$, which is defined by equation (4), is shown in Fig. 4(*b*). At $r = 0$, $f(r)$ is unity and it linearly decreases with r in the region $0 < r < t$.

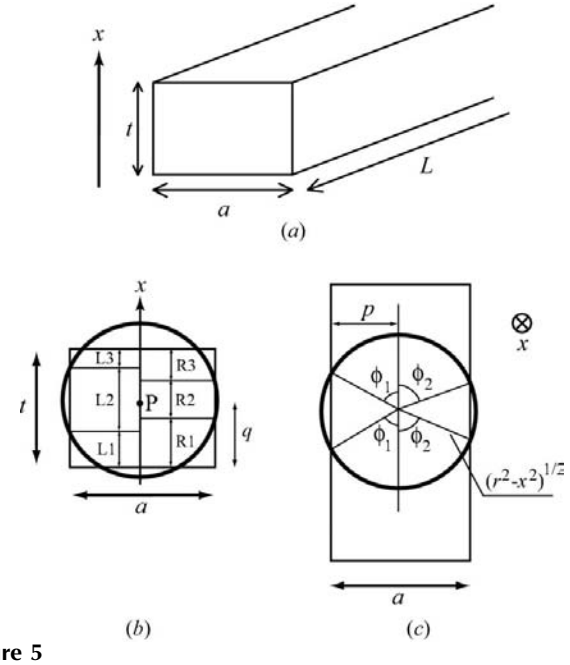

Figure 5
(*a*) Three-dimensional scheme of nanobelt with width a and thickness t. (*b*) Sectioned diagram of the nanobelt. (*c*) View along the x direction.

2.4. Nanobelt

We consider a nanobelt with a width a and a thickness t, as shown in Fig. 5. Let the length of the belt L be much longer than r. Fig. 5(*b*) shows a sectioned diagram of the belt. The center of the circle (P) in the figure is at distances p from the left wall and q from the bottom wall. The PRDF at (p, q), $R(r, p, q)$, is proportional to the surface area of the part of the sphere that crosses the belt. The surface area of the object obtained by rotating by $\phi(x)$ around the x axis with radius $y(x)$ is obtained by $S = \int\int_{\phi(x)} y(x)\,\mathrm{d}\phi\,\mathrm{d}s$, where $\mathrm{d}s = (dx^2 + dy^2)^{1/2}$. In the case of a sphere, $y = (r^2 - x^2)^{1/2}$ and $S = \int r\phi(x)\,\mathrm{d}x$. Here, we calculate $R(r, p, q)$ by separating six parts, L1–L3, R1–R3, as shown in Fig. 5(*b*). The surface area of L2 is obtained by the rotation from zero to $\phi_1(x)$ and from $\pi - \phi_1(x)$ to π, and the area of R2 is obtained by the rotation from zero to $\phi_2(x)$ and from $\pi - \phi_2(x)$ to π, as shown in Fig. 5(*c*). The surface areas of the other parts are obtained by the rotation of π. Then $R(r, p, q)$ is given by

$$R(r,p,q) = \rho'_{0,\mathrm{3D}}\left[\int_{\mathrm{L1}} \pi r\,\mathrm{d}x + \int_{\mathrm{L2}} 2\phi_1(x) r\,\mathrm{d}x + \int_{\mathrm{L3}} \pi r\,\mathrm{d}x + \int_{R1} \pi r\,\mathrm{d}x + \int_{\mathrm{R2}} 2\phi_2(x) r\,\mathrm{d}x + \int_{\mathrm{R3}} \pi r\,\mathrm{d}x\right]. \quad (10)$$

The direction of the x axis is shown in Fig. 5(*b*) and the origin of the x axis is the center of the corresponding sphere. $\phi_1(x)$ and $\phi_2(x)$ are given by

$$\phi_1(x) = \arcsin\frac{p}{(r^2 - x^2)^{1/2}},$$
$$\phi_2(x) = \arcsin\frac{a - p}{(r^2 - x^2)^{1/2}},$$

as shown in Fig. 5(*c*). The integral ranges in equation (10) depend on the relations between r, t, a, p and q. The integral ranges of the left side (L1, L2 and L3) for various conditions of the above parameters are shown in Table 1. For R1, R2 and R3, the integral ranges are obtained by substituting $a - p$ for p in the table. The case shown in Fig. 5(*b*) corresponds to the condition $r > p$, $(r^2 - p^2)^{1/2} < q < r$ and $t - r < q < t - (r^2 - p^2)^{1/2}$. Because the integrations for the range L2 and R2 cannot be calculated analytically, they are obtained by numerical calculations. $R_{\mathrm{belt}}(r)$ is given by

$$R_{\mathrm{belt}}(r) = \int_0^a \int_0^t R(r,p,q)\,\mathrm{d}q\,\mathrm{d}p/(ta).$$

The RDFs calculated for the nanobelts with various thicknesses t are shown in Fig. 6(a).

For $r \gg a, t$, $R_{\rm belt}(r)$ becomes flat and it is proportional to $at\rho'_{0,3D}$, corresponding to $R_{1D}(r)$. The correction factors obtained by equation (4) are shown in Fig. 6(b). At $r \sim 0$, $f_{\rm belt}(r)$ for $t = a$ and $t = a/2$ are slightly larger than unity, owing to the insufficiency of the accuracy of the numerical calculation.

2.5. Nanorod and nanotube

In this subsection, first we consider the nanorod as shown in Fig. 7(a). We also assume that $r \ll L$. Fig. 7(b) shows a sectioned diagram. We consider the surface area of the overlapping part of the sphere with radius r and the rod with radius a. The center of the sphere is distant from the center of the rod by PA = p. The PRDF at p, $R(r, p)$, is proportional to the surface area. It is similar to the cases of the nanosheet and the nanobelt. $R(r, p)$ is obtained as

$$R(r,p) = \left[\int_{\rm I1} 4\phi(x) r\,{\rm d}x + \int_{\rm I2} 2\pi r\,{\rm d}x\right]\rho'_{0,3D},$$

where $\phi(x)$ is given by

$$\phi(x) = \arcsin\left[\frac{a^2-(x-p)^2}{r^2-x^2}\right]^{1/2},$$

as shown in Fig. 7(c). The integral ranges I1 and I2 depend on the relation between the parameters a, r and p. First, the case of $r < a$ is considered. In this case, when $p - a < -r$, the sphere is perfectly enveloped in the rod. If $p - a > -r$, the integral range on x is divided into two as I1: $p - a \le x \le r\cos\alpha$ and I2: $r\cos\alpha \le x \le r$, where $\cos\alpha = [(p^2 + r^2 - a^2)/2pr]$. Then $R(r, p)$ is given, for $r < a$, by

$$R(r,p) = \begin{cases} 4\pi r^2 \rho'_{0,3D} & (p \le a - r) \\ \left[\int\limits_{p-a}^{r\cos\alpha} 4\phi(x) r\,{\rm d}x + \int\limits_{r\cos\alpha}^{r} 2\pi r\,{\rm d}x\right]\rho'_{0,3D} & \\ \quad = \left\{4r\int\limits_{p-a}^{r\cos\alpha} \arcsin\left[\frac{a^2-(x-p)^2}{r^2-x^2}\right]^{1/2} {\rm d}x \right. & \\ \quad \left. + 2\pi r^2\left(1 - \frac{p^2+r^2-a^2}{2pr}\right)\right\}\rho'_{0,3D} & \\ & (p \ge a - r). \end{cases} \tag{11}$$

Since the RDF is given by $\int_0^a R(r,p) 2\pi p\,{\rm d}p/\pi a^2$, $R_{\rm rod}(r)$ is obtained from the above equations as

$$\begin{aligned} R_{\rm rod}(r) = {} & \rho'_{0,3D}\int_0^{a-r} 4\pi r^2 2\pi p\,{\rm d}p/\pi a^2 \\ & + \rho'_{0,3D}\int_{a-r}^{a}\left\{2\pi r^2\left(1 - \frac{p^2+r^2-a^2}{2pr}\right)2\pi p \right. \\ & \left. + 4r\int\limits_{p-a}^{r\cos\alpha} \arcsin\left[\frac{a^2-(x-p)^2}{r^2-x^2}\right]^{1/2} {\rm d}x\right\} \\ & \times 2\pi p\,{\rm d}p/\pi a^2 \quad (r < a). \end{aligned} \tag{12}$$

The integration over x needs a numerical calculation.

In the case of $r > a$, $R(r, p)$ can be given by the second formula in equation (11) when $p + a > r$. When $p + a < r$, the circle with radius a, which corresponds with a section of the rod, is completely enveloped by the circle with radius r. Then $R(r, p)$ is given by

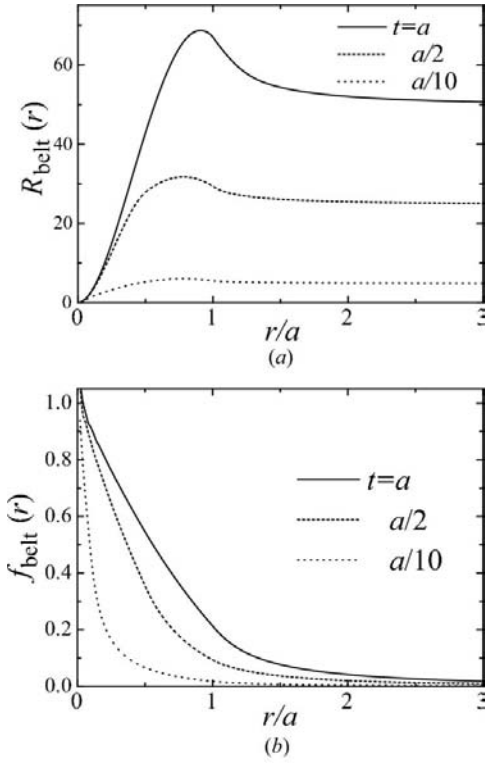

Figure 6
(a) The radial distribution functions and (b) the correction factors of the nanobelts with various t.

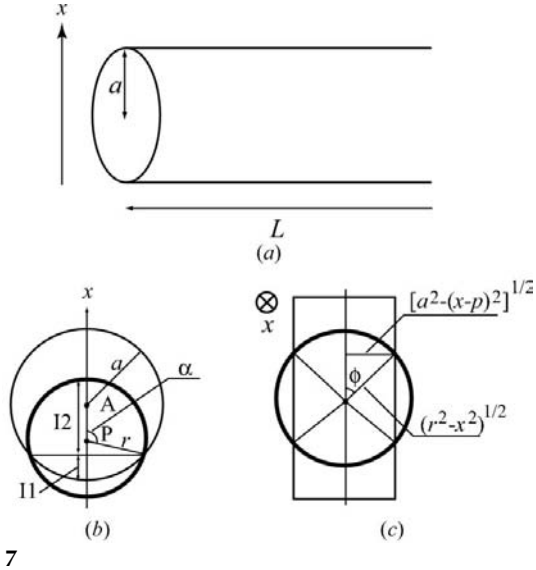

Figure 7
(a) Nanorod with radius a. (b) Sectioned diagram of the nanorod whose center is at A. (c) View along the x direction.

$$R(r,p) = \rho'_{0,3D}\int_{p-a}^{p+a} 4\phi(x) r\,\mathrm{d}x = 4r\rho'_{0,3D}\int_{p-a}^{p+a} \arcsin\left(\frac{a^2-(x-p)^2}{r^2-x^2}\right)^{1/2}\mathrm{d}x. \quad (13)$$

As a result, for $r > a$, $R_{\rm rod}$ is obtained as

$$\begin{aligned} R_{\rm rod}(r) = {} & \rho'_{0,3D}\int_0^{r-a}\int_{p-a}^{p+a} 4r\arcsin\left[\frac{a^2-(x-p)^2}{r^2-x^2}\right]^{1/2}\mathrm{d}x \\ & \times 2\pi p\,\mathrm{d}p/\pi a^2 \\ & + \rho'_{0,3D}\int_{r-a}^{a}\left\{2\pi r^2\left(1-\frac{p^2+r^2-a^2}{2pr}\right)\right. \\ & \left. + 4r\int_{p-a}^{r\cos\alpha}\arcsin\left[\frac{a^2-(x-p)^2}{r^2-x^2}\right]^{1/2}\mathrm{d}x\right\} \\ & \times 2\pi p\,\mathrm{d}p/\pi a^2 \quad (r \geq a). \end{aligned} \quad (14)$$

The integrations over x included in the first and the third terms are calculated numerically.

Next, we consider a nanotube shown in Fig. 8. The external and internal diameters are $2a$ and $2b$, respectively. In the calculation, we consider the PRDFs at p for the nanorod, $R_a(r,p)$ and $R_b(r,p)$, where p is the distance between the center of the tube and the sphere with radius r. The RDF of the nanotube is given by using $R_a(r,p)$ and $R_b(r,p)$, as follows.

$$R_{\rm tube}(r) = \int_b^a [R_a(r,p) - R_b(r,p)]2\pi p\,\mathrm{d}p/\pi(a^2-b^2). \quad (15)$$

$R_a(r,p)$ can be calculated in the same way as the case of the rod. $R_b(r,p)$ can be given for the conditions of the parameters as

$$R_b(r,p) = \begin{cases} 4r\rho'_{0,3D}\displaystyle\int_{p-b}^{p+b}\arcsin\left[\frac{b^2-(x-p)^2}{r^2-x^2}\right]^{1/2}\mathrm{d}x & (p \leq r-b) \\ \rho'_{0,3D}\left\{2\pi r^2\left(1-\dfrac{p^2+r^2-b^2}{2pr}\right)\right. & \\ \quad \left. + 4r\displaystyle\int_{r\cos\alpha}^{p-b}\arcsin\left[\frac{b^2-(x-p)^2}{r^2-x^2}\right]^{1/2}\mathrm{d}x\right\} & (p \geq r-b) \\ 0 & (p \geq r+b). \end{cases} \quad (16)$$

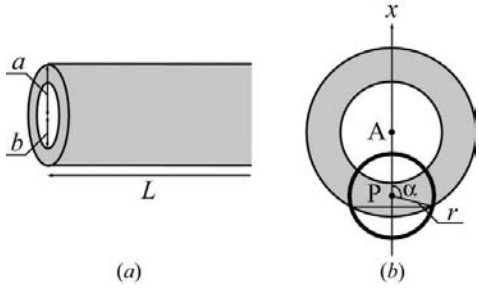

Figure 8
(*a*) Nanotube with external diameter $2a$ and an internal diameter $2b$. (*b*) Sectioned diagram of the nanotube.

By using the above equations, we calculate the RDFs of the nanorod and the nanotubes, as shown in Fig. 9(*a*). In these figures, we define a thickness $t = a - b$. The atomic number densities in the rod and the tubes, $\rho'_{0,3D}$, are unity. At $r \gg a, t$, the RDFs have constant values which correspond with a product of the sectioned area and the density. It is the same as the case of the nanobelt. $R_{\rm tube}(r)$ with small thicknesses have sharp peaks at $r \sim 2a$. The correction factors $f_{\rm tube}(r)$ are shown in Fig. 9(*b*). The correction factor of the tube decreases with r and has a shoulder at $r \sim 2a - t$.

2.6. Sphere

In this subsection, the RDFs for the sphere and the spherical shell are calculated. First, the filled sphere with radius a as shown in Fig. 10(*a*) is considered. In this case, we consider $R(r,p)$, where p is the length PA shown in Fig. 10. In the case of $r < a$, it can be obtained as

$$R(r,p) = \begin{cases} 4\pi r^2\rho'_{0,3D} & (p \leq a-r) \\ \rho'_{0,3D}\displaystyle\int_{r\cos\alpha}^{r} 2\pi r\,\mathrm{d}x & \\ \quad = 2\pi r^2\rho'_{0,3D}\left(1-\dfrac{p^2+r^2-a^2}{2pr}\right) & (p \geq a-r). \end{cases} \quad (17)$$

In the case of $a < r < 2a$,

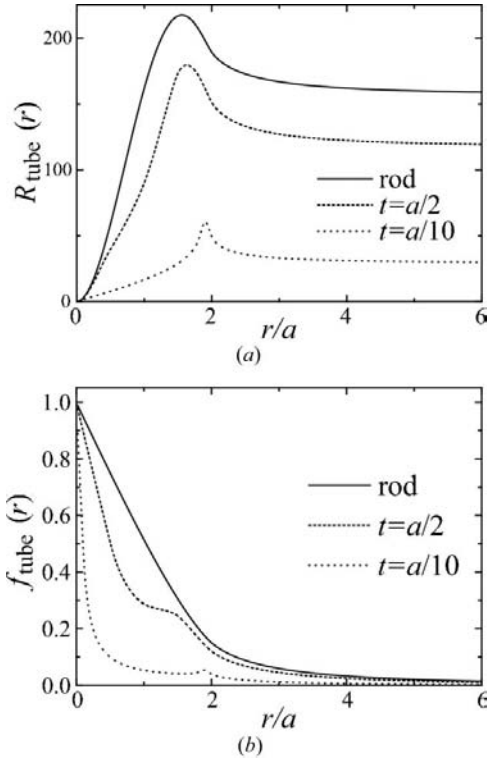

Figure 9
(*a*) The radial distribution functions and (*b*) the correction factors of the nanorod and the nanotubes with various t.

$$R(r,p)=\begin{cases}0 & (p\le r-a)\\ \rho'_{0,3D}\int\limits_{r\cos\alpha}^{r}2\pi r\,\mathrm{d}x & \\ \quad=2\pi r^2\rho'_{0,3D}\left(1-\dfrac{p^2+r^2-a^2}{2pr}\right) & (p\ge r-a).\end{cases}\tag{18}$$

For $r>2a$, $R(r,p)=0$. The RDF can be given by

$$R_{F\mathrm{sphere}}(r)=\frac{\int_0^a R(r,p)4\pi p^2\,\mathrm{d}p}{\frac{4}{3}\pi a^3}.\tag{19}$$

The above integrations of equations (17) and (18) give the same results. Then,

$$R_{F\mathrm{sphere}}(r)=\begin{cases}\pi r^2\rho'_{0,3D}\left[\frac{1}{4}\left(\frac{r}{a}\right)^3-3\frac{r}{a}+4\right] & (r\le 2a)\\ 0 & (r>2a).\end{cases}\tag{20}$$

The finite size effect or the correction factor of the spherical case has already been calculated by Mason (1968). This was for the estimation of the RDF and the coordination numbers of balls packed in a finite sphere, in order to discuss atoms in liquids and not for the RDF of nanoparticles. The present result is consistent with his.

In the case of the spherical shell with a thickness $t=a-b$ shown in Fig. 10(b), we consider the PRDF at p for the filled spheres with radii a and b, $R_a(r,p)$ and $R_b(r,p)$, respectively, and the RDF can be given by

$$R_{E\mathrm{sphere}}(r)=\frac{\int_b^a\left[R_a(r,p)-R_b(r,p)\right]4\pi p^2\,\mathrm{d}p}{\frac{4}{3}\pi(a^3-b^3)}.\tag{21}$$

$R_a(r,p)$ corresponds with equations (17) and (18). $R_b(r,p)$ is obtained as

$$R_b(r,p)=\begin{cases}0 & (p<r-b)\\ 2\pi r^2\rho'_{0,3D}\left(1-\dfrac{p^2+r^2-b^2}{2pr}\right) & \\ & (r-b\le p\le r+b)\\ 0 & (p>r+b).\end{cases}\tag{22}$$

By using equations (17), (18), (21) and (22), the RDFs for the spherical shells with various t are calculated by using $\rho_{0,3D}=1$, as shown in Fig. 11(a). The correction factors are shown in Fig. 11(b).

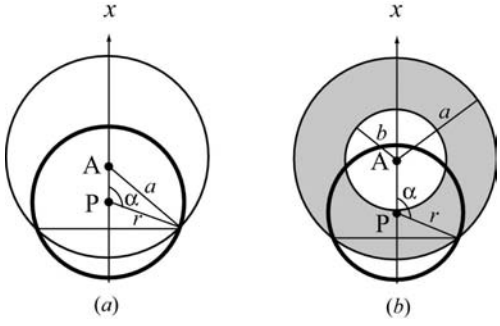

Figure 10
Sectioned diagram of (a) filled sphere and (b) spherical shell with external and internal radii a and b, respectively.

3. Formulation of the finite size effect for PDF analysis

In this section, we present the formulation of the PDF analysis which takes account of the finite size effect of a nanoparticle. In the previous section, we neglect the atomic pair distribution between the particles. Here, we consider the partial radial distribution function including the atomic pair distributions not only inside a particle but also between the particles. It is assumed that the nanoparticles are in vacuum. Each particle is distributed randomly and there is no atomic correlation between the particles. In this assumption, the atomic distribution outside the particle can be regarded as being continuous with a density of ρ_0, which corresponds with the density averaged in the whole sample including all particles and the space between them. The atomic arrangement inside a particle is periodic and uniform with a density of ρ'_0 in a whole particle (we neglect, for example, the rearrangement of the surface atoms). Here we rewrite the radial distribution and the partial radial distribution functions obtained for a single particle made of atoms as $R_{\mathrm{nano}}(r)$ and $R_{\mathrm{nano}}(r,p)$ [or $R_{\mathrm{nano}}(r,p,q)$], respectively. Then the partial radial distribution function $R(r,p)$ [or $R(r,p,q)$] is given as follows.

$$R(r,p)=R_{\mathrm{nano}}(r,p)+[4\pi r^2-S_{\mathrm{nano}}(r,p)]\rho_0,$$

where $S_{\mathrm{nano}}(r,p)$ shows a surface area of the sphere with a radius r centered at P inside the particle. In the above equation, the first term shows the pair distribution inside the particle, whereas the second term shows the pair distribution outside the particle (the pair distribution between the

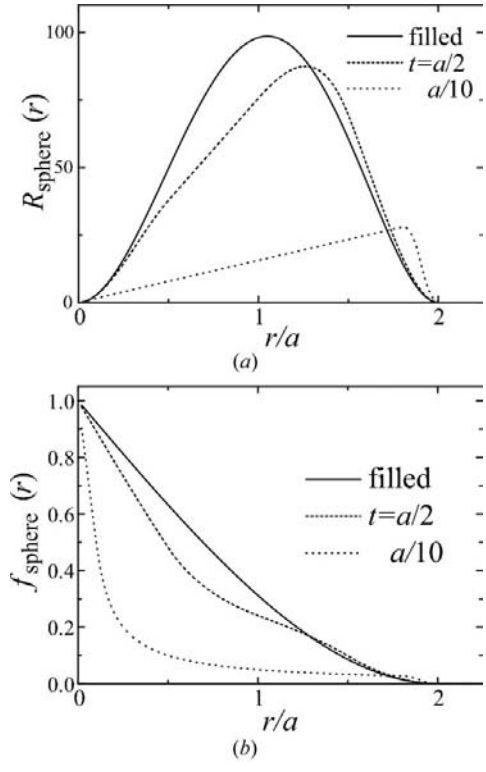

Figure 11
(a) The radial distribution functions and (b) the correction factors of the nanospheres with various t.

particles). If the nanoparticle consists of continua, $R_{\rm nano}(r,p)/\rho_0'$ becomes equal to $S_{\rm nano}(r,p)$. Then the radial distribution function is given by

$$R(r) = R_{\rm nano}(r) + [4\pi r^2 - S_{\rm nano}(r)]\rho_0,$$

where $S_{\rm nano}(r)$ is the surface area inside the particle averaged by p. Since $S_{\rm nano}(r)$ is $4\pi r^2 f(r)$, the RDF can be represented as

$$R(r) = f(r)R_\infty(r) + 4\pi r^2\rho_0[1 - f(r)], \tag{23}$$

where $R_\infty(r)$ is the RDF of the bulk sample with infinite size. Here we use equation (4) for the first term. For the bulk sample, the PDF and the reduced PDF are given by

$$\begin{aligned} g_\infty(r) &= R_\infty(r)/4\pi r^2\rho_0', \\ G_\infty(r) &= 4\pi r\rho_0'[g_\infty(r) - 1], \end{aligned} \tag{24}$$

where $g_\infty(r)$ and $G_\infty(r)$ are the PDF and the reduced PDF of the bulk sample. From equations (1), (2), (23) and (24), the PDF and the reduced PDF are represented as

$$g(r) = \frac{\rho_0'}{\rho_0}f(r)g_\infty(r) + 1 - f(r), \tag{25}$$

$$G(r) = f(r)G_\infty(r) + 4\pi r(\rho_0' - \rho_0)f(r). \tag{26}$$

In the case of the isotropic scattering in a sample with infinite size, the structure function $S(Q)$ is generally given using $g(r)$ as

$$\begin{aligned} S(Q) &= 1 + \int 4\pi r^2\rho_0 g(r)\frac{\sin(Qr)}{Qr}\,{\rm d}r, \\ &= 1 + \int 4\pi r^2\rho_0[g(r) - 1]\frac{\sin(Qr)}{Qr}\,{\rm d}r \\ &\quad + \int 4\pi r^2\rho_0\frac{\sin(Qr)}{Qr}\,{\rm d}r. \end{aligned} \tag{27}$$

This equation leads to the general relation between $S(Q)$ and $G(r)$ shown in equation (3). By substituting equation (25) into equation (27), and by using equation (24), we can obtain the $S(Q)$ for nanoparticles:

$$\begin{aligned} S(Q) &= 1 + \int 4\pi r^2\rho_0'[g_\infty(r) - 1]\frac{\sin(Qr)}{Qr}\,{\rm d}r \\ &\quad + \int 4\pi r^2(\rho_0' - \rho_0)f(r)\frac{\sin(Qr)}{Qr}\,{\rm d}r \\ &\quad + \int 4\pi r^2\rho_0\frac{\sin(Qr)}{Qr}\,{\rm d}r \\ &= 1 + \frac{1}{Q}\int f(r)G_\infty(r)\sin(Qr)\,{\rm d}r \\ &\quad + \frac{1}{Q}\int 4\pi r(\rho_0' - \rho_0)f(r)\sin(Qr)\,{\rm d}r \\ &\quad + \int 4\pi r^2\rho_0\frac{\sin(Qr)}{Qr}\,{\rm d}r. \end{aligned} \tag{28}$$

In equations (27) and (28), the third and the fourth terms, respectively, are neglected because of overlapping with the direct beam. In the cases of nanoparticles, the third term of equation (28) appears in comparison with the case of the bulk [equation (27)]. This term corresponds to the Fourier transform of the second term of equation (26). The second term of equation (26) is independent of the arrangement of the atoms inside the nanoparticle and depends only on the shape and the size of the nanoparticles (and the densities), while the first term depends on both the atomic arrangement in the nanoparticles and the shape and the size of the nanoparticles. Then the third term of equation (28) has a structure only in the small-Q region, corresponding to small-angle scattering.

In the conventional PDF analysis for a solid sample, the data of $S(Q)$ in such a small Q region are not used and $S(Q)$ is regarded as zero in the limit of $Q \to 0$. Here we represent the structure function as a superposition of two parts, $S(Q) = S_S(Q) + S_L(Q)$, where $S_L(Q)$ is the structure function used in conventional PDF analysis and $S_S(Q)$ is the function which has a structure only in the small-Q region, as follows.

$$\begin{aligned} S_L(Q) &= 1 + \frac{1}{Q}\int f(r)G_\infty(r)\sin(Qr)\,{\rm d}r, \\ S_S(Q) &= \frac{1}{Q}\int 4\pi r(\rho_0' - \rho_0)f(r)\sin(Qr)\,{\rm d}r. \end{aligned}$$

From the inverse Fourier transforms of the above equations, we can obtain

$$f(r)G_\infty(r) = \frac{2}{\pi}\int Q[S_L(Q) - 1]\sin(Qr)\,{\rm d}Q, \tag{29}$$

$$4\pi r(\rho_0' - \rho_0)f(r) = \frac{2}{\pi}\int QS_S(Q)\sin(Qr)\,{\rm d}Q. \tag{30}$$

In the analysis of a nanoparticle without small-angle-scattering data, we may use equation (29) and modify the reduced PDF by the relation

$$G(r) = f(r)G_\infty(r). \tag{31}$$

As a result, the reduced PDF of a nanoparticle may be described by a product of the correction factor and the reduced PDF of the bulk sample. The same relation is reached

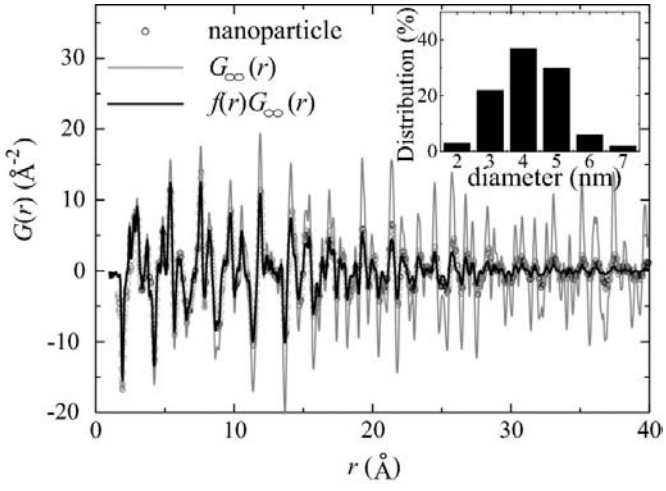

Figure 12
The reduced PDF of anatase TiO_2 nanoparticles obtained by neutron diffraction is shown by open circles. The gray and black lines show the reduced PDF of bulk TiO_2 and that modified by equation (31), respectively. The inset shows the distribution of the diameter of the anatase TiO_2 nanoparticles.

by another method without the pair distribution between particles (Azaroff *et al.*, 1972).

4. Application to experimental data

In this section, we apply the obtained equations to the experimental data on anatase-type TiO_2 nanoparticles. The shape of the particle is almost spherical and the distribution of the diameter is shown in the inset of Fig. 12. It is determined by the transmission-electron-microscope image. The diffraction data are collected at the neutron powder diffractometer NPDF (Proffen *et al.*, 2002) in the Manuel Lujan Neutron Scattering Center of Los Alamos National Laboratory. The data in the range $1.65 < Q < 45$ Å^{-1} are transformed into the reduced PDF $G(r)$ by using the program *PDFgetN* (Proffen & Billinge, 1999). The obtained $G(r)$ is shown in the main panel of Fig. 12 by open circles. The gray line in the figure shows $G_\infty(r)$, which is obtained from the diffraction data of the bulk sample of anatase TiO_2 with an average diameter of ~200 nm. The diffraction data of the bulk sample are collected under the same experimental conditions. The peak intensities of $G(r)$ of the nanoparticle are apparently damped with increasing r, in comparison with the intensities of $G_\infty(r)$. The black line shows the reduced PDF obtained by using equation (31). Here we use the correction factor $f(r)$ which takes account of the diameter distribution,

$$f(r) = \sum_d N_d f_d(r), \tag{32}$$

where N_d is the percentage of the nanoparticles with diameter d, shown in the inset of Fig. 12. $f_d(r)$ is the correction factor for a spherical nanoparticle with diameter d, which is given by equation (20). The modified $G(r)$ can reproduce the observed data in the whole r region. We can conclude that our modified formula is valid for the PDF analysis of nanoparticles.

5. Discussion

In this article, we consider the finite size effects of nanoparticles on the PDF analysis. On the other hand, studies on diffraction by small crystalline particles were performed widely in 1930s (for example, Patterson, 1939). In these studies, the effects of the sizes and shapes of the particles on the diffraction peaks were discussed. Patterson gave the diffraction pattern as the convolution of the structure factor and the shape function which depends on the particle shape (Patterson, 1939). He basically calculated the shape function for the tetrahedron and, for other polyhedrons, the shape functions were obtained as sums of the functions of their constituent tetrahedra. His calculations were performed in the reciprocal-lattice space and the shape functions were given as functions of the reciprocal-lattice vector. Our calculations, on the other hand, are performed in the real space and the correction factor is a function only of the distance in the real space. While the method and obtained functions by Patterson are different from those of our calculation, the shape function should be essentially related to the correction factor. If the shape functions can be averaged for all directions (powder averaged), they should be related to the scattering functions of small-angle scattering, which are related to the correction factors by equation (30).

We present the correction factors for various shapes of nanoparticles and the modified formulas of PDF analysis with the correction factor. These results enable us to determine the crystal structure of nanoparticles and/or their shape and size. Usually, the shape and the size of the particles are determined by small-angle scattering. In the small-angle-scattering measurement, because the wavevector is much smaller than the inverse of the atomic scale, and thus the particle can be regarded as a continuum, the scattering profile depends on the shape and the size of the particle and is independent of the structural coherence inside the particle. In the PDF analysis, $G_\infty(r)$ of the continuum is zero, which is obtained from the equation $R_\infty(r) = 4\pi r^2 \rho_0'$ and equation (24). Then the reduced PDF strongly depends on the structural coherence in the particle. It can cause a discrepancy between the particle sizes estimated by the PDF analysis and small-angle scattering, and such a discrepancy gives us information about local lattice disorder in the nanoparticle. Gilbert *et al.* (2004) have shown that the PDF profile of a zinc sulfide nanoparticle decreases with r more rapidly than the profile expected from the shape and size of the particle which are determined by the small-angle scattering. They pointed out that the reduction of the PDF profile is due to the local structural disorder driven by the strain in the particle. In addition, they estimated the structural coherence length. They speculate that the strain is caused by the irregular surface. The PDF analysis which takes account of the finite size effect of nanoparticles enable us not only to determine the crystal structure but also to estimate the local lattice disorder in nanoparticles.

6. Conclusions

PDFs for various nanoparticles strongly depend on their shapes and sizes. The modified equation of the reduced PDF including the finite size effect of a nanoparticle is described by a simple formula, a product of the correction factor for the shape and the size of the particle and the reduced PDF of a bulk sample. It is confirmed that the modified formula actually reproduces the experimental reduced PDF of TiO_2 nanoparticles. This analysis also enables us to discuss the local lattice disorder included in the nanoparticle.

The authors thank Professor S. Sinha for fruitful discussions. This work was supported by a Grant-in-Aid for Scientific Research from the Ministry of Education, Culture, Sports, Science and Technology of Japan. This work has benefited from the use of NPDF at the Lujan Center at Los Alamos Neutron Science Center. Los Alamos National Laboratory is funded by DOE under Contract No. W-7405-ENG-36. The upgrade of NPDF has been funded by NSF through Grant No. DMR 00-76488.

References

Azaroff, L. V., Kaplow, R., Kato, N., Weiss, R. J., Wilson, A. J. C. & Young, R. A. (1972). *X-ray Diffraction*. New York: McGraw-Hill.

Egami, T. & Billinge, S. J. L. (2003). *Underneath the Bragg Peaks. Structural Analysis of Complex Materials*. Amsterdam: Pergamon.

Gateshki, M., Hwang, S.-J., Park, D. H., Ren, Y. & Petkov, V. (2004). *J. Phys. Chem.* B**108** 14956–14963.

Gilbert, B., Huang, F., Zhang, H., Waychunas, G. A. & Banfield, J. F. (2004). *Science*, **305**, 651–654.

Mckenzie, D. R., Davis, C. A., Cockayne, D. J. H., Muller, D. A. & Vassallo, A. M. (1992). *Nature (London)*, **355**, 622–624.

Mason, G. (1968). *Nature (London)*, **217**, 733–734.

Patterson, A. L. (1939). *Phys. Rev.* **56**, 972–977.

Petkov, V., Zavalij, P. Y., Lutta, S., Whittingham, M. S., Parvanov, V. & Shastri, S. (2004). *Phys. Rev. B*, **69**, 85410.

Proffen, T. & Billinge, S. J. L. (1999). *J. Appl. Cryst.* **32**, 572–575.

Proffen, T., Egami, T., Billinge, S. J. L., Cheetham, A. K., Louca, D. & Parise, J. B. (2002). *Mater. Sci. Process.* **74**, S163–S165.